Letter | Editors' Suggestion

Rapidity and momentum distributions of one-dimensional dipolar quantum gases

Kuan-Yu Li,[1,2,*] Yicheng Zhang,[3,4,5,*] Kangning Yang,[2,6] Kuan-Yu Lin,[2,6] Sarang Gopalakrishnan,[3,7] Marcos Rigol,[3] and Benjamin L. Lev[1,2,6]

[1]*Department of Applied Physics, Stanford University, Stanford, California 94305, USA*
[2]*E. L. Ginzton Laboratory, Stanford University, Stanford, California 94305, USA*
[3]*Department of Physics, Pennsylvania State University, University Park, Pennsylvania 16802, USA*
[4]*Homer L. Dodge Department of Physics and Astronomy, The University of Oklahoma, Norman, Oklahoma 73019, USA*
[5]*Center for Quantum Research and Technology, The University of Oklahoma, Norman, Oklahoma 73019, USA*
[6]*Department of Physics, Stanford University, Stanford, California 94305, USA*
[7]*Department of Electrical and Computer Engineering, Princeton University, Princeton, New Jersey 08544, USA*

(Received 17 November 2022; revised 29 January 2023; accepted 22 May 2023; published 8 June 2023)

We explore the effect of tunable integrability-breaking dipole-dipole interactions in the equilibrium states of highly magnetic one-dimensional (1D) Bose gases of dysprosium at low temperatures. We experimentally observe that in the strongly correlated Tonks-Girardeau regime, rapidity and momentum distributions are nearly unaffected by the dipolar interactions. By contrast, we also observe that significant changes of these distributions occur when decreasing the strength of the contact interactions. We show that the main experimental observations are captured by modeling the system as an array of 1D gases with only contact interactions, dressed by the contribution of the short-range part of the dipolar interactions. Improvements to theory-experiment correspondence will require different tools tailored to near-integrable models possessing both short- and long-range interactions.

DOI: 10.1103/PhysRevA.107.L061302

One-dimensional (1D) bosonic gases with only contact interactions are *integrable*, and, consequently, they possess stable quasiparticles [1]. Integrability is in general unstable to the addition of long-range interactions. Even weak integrability-breaking interactions have drastic effects on the nonequilibrium dynamics of integrable systems, causing relaxation to a thermal distribution: For dipole-dipole interactions (DDIs) these dynamical effects were recently explored [2]. By contrast, the effects of integrability-breaking interactions on equilibrium states are less clear: Instead of causing quasiparticles to decay, one might expect (in the spirit of Fermi-liquid theory) that interactions simply perturbatively dress the quasiparticles. When the energy scale associated with integrability breaking is a small fraction of the other natural energy scales, it is plausible that the dressing will be weak and the bare quasiparticles can still provide an accurate description. This expectation has not been experimentally tested so far; it is not *a priori* clear how the dressing depends on the parameters of the integrable system and on the type of integrability-breaking interaction.

In the past, characterizing the dressing of quasiparticles would have been a forbidding experimental challenge: In dense, strongly interacting systems, the mapping between quasiparticles and microscopic particles is nontrivial, and the quantum numbers of the quasiparticles (known as rapidities) are distinct from the microscopic particle momenta, making their distribution hard to measure [3,4]. In a recent experimental breakthrough, a modified time-of-flight (TOF) sequence was developed to measure the rapidity distribution of 1D gases [5,6]. In this protocol, one first allows the system to freely expand in 1D under near-integrable dynamics; this step preserves the rapidity distribution. Once the system is dilute, rapidity and momentum distributions coincide, and one can extract the rapidity distribution via TOF imaging.

Here, we use measurements of rapidity and momentum distributions in an array of 1D bosonic gases with a tunable DDI to explore how the DDI affects the equilibrium properties, e.g., via a dressing of the quasiparticles, and how the effect of the DDI varies when changing the strength of the contact interactions. We find that both distributions are nearly unaffected by the DDI in the Tonks-Girardeau (TG) regime, suggesting that the bare quasiparticles can be used to characterize that regime. As the strength of the contact interactions is decreased, the densities of the 1D gases increase and with them the strength of the dipolar interactions. We find that, as a result, the dressing of the quasiparticles becomes significant and needs to be taken into account in any model of the system in that regime. To attempt to do so, we confirm that modeling the system as an array of 1D gases with only (integrable) contact interactions (dressed with the short-range part of the DDI) is most accurate in the TG regime. We also show that the model captures the experimental trends as the strength of the contact interactions is decreased. A more accurate correspondence will require the development of different theoretical tools to account for the long-range part of the dipolar interaction and dynamical effects during the initial state preparation.

A dipolar ^{162}Dy BEC of $2.3(1) \times 10^4$ atoms is prepared in a 1064-nm crossed optical dipole trap (ODT) with a final trap

*These authors contributed equally to this work.

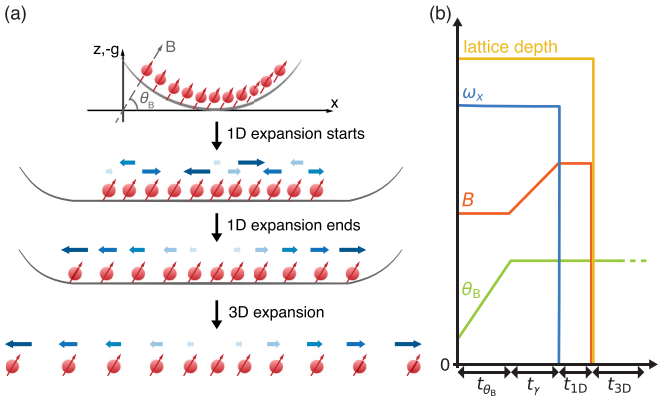

FIG. 1. (a) Schematic illustrating the experimental sequence for measuring the rapidity distribution of a dipolar 1D gas. A dipolar 1D gas is prepared with a magnetic field magnitude B and angle θ_B resulting in contact strength g_{1D}. Then, the underlying harmonic trap is suddenly removed, while the transverse confinement is maintained. This allows the quantum gas to expand in a flat, 1D trap along $\hat{x}$. Time-of-flight absorption imaging follows 3D expansion by switching off all optical traps. The blue arrows denote the rapidities. (b) Timing sequence for creating a dipolar 1D gas at dipolar angle θ_B and g_{1D}. Once the quantum gas is loaded into a quasi-1D trap, the B-field angle is slowly rotated from 55° to $\theta_B = 0°$, 35°, or 90° in a time t_{θ_B}, or kept at 55°, as the experiment requires. g_{1D} is then set to its final value by ramping the B-field strength near a Feshbach resonance in a time $t_\gamma = 50$ ms.

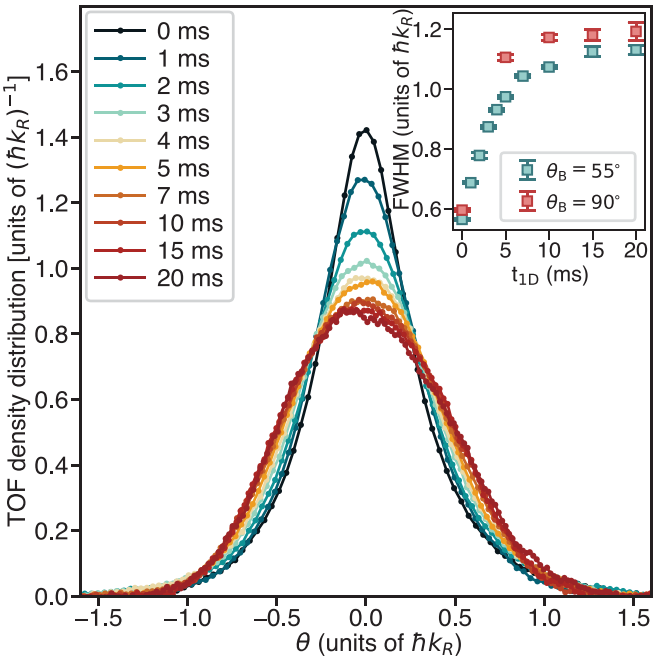

FIG. 2. The TOF density distribution for $\theta_B = 55°$ and $\gamma_T \approx 16$ for $t_{1D} = 0$–20 ms. The width of the distributions' θ has been scaled by $\hbar k_R$. Data at times >15 ms suffer from imaging artifacts and are not used. Inset: The evolution of the FWHM of the distribution vs t_{1D} for $\gamma_T \approx 16$ at $\theta_B = 55°$ (light green) and $\gamma_T \approx 19$ at $\theta_B = 90°$ (red). Error bars are explained in Ref. [8].

frequency of $2\pi \times [55.5(6), 22.5(5), 119.0(7)]$ Hz; more details can be found in Refs. [2,7]. The gas is then adiabatically loaded into a 2D optical lattice that is blue-detuned from Dy's 741-nm transition [8,9]. Roughly two thousand 1D traps are populated, with the central ones containing about 40 atoms. Before loading, the angle of an externally imposed magnetic field is set to $\theta_B \approx 55°$ with respect to $\hat{x}$, the 1D axis of the gases. This minimizes the intratube DDI among atoms within the same 1D trap, which scales as $1 - 3\cos^2\theta_B$. When the optical lattice reaches a depth of $30E_R$, the 1D trap frequency ω_x is lowered to $2\pi \times 36.4(3)$ Hz by reducing the power of the 1064-nm ODT. The recoil energy is $E_R = \hbar^2 k_R^2/2m$ and $k_R = 2\pi/741$ nm, where m is the mass of the highly magnetic, 10 Bohr magneton ^{162}Dy atom we use [10]. Simultaneously, a 1560-nm ODT is superimposed to negate the antitrapping potential caused by the blue-detuned optical lattice. We then set θ_B to the particular value we require by rotating the magnetic field while maintaining the same lattice depth by adjusting the optical lattice power to compensate for the large tensor light shift [9]. The 1D-regularized contact interaction strength g_{1D} is then ramped to the required final value via a confinement-induced resonance [7,11,12]. The resonance is accessed by adjusting the magnitude B of the magnetic field near a Feshbach resonance [8,13]. To create the dilute TG gases, we prepare a smaller BEC of $5.8(2) \times 10^3$ atoms and set $\theta_B = 90°$; this leads to a maximum of about 15 atoms in the central 1D tubes.

Figure 1 illustrates the experimental sequence for measuring rapidity and momentum distributions. The rapidity distribution is measured using a 1D expansion of duration $t_{1D} = 15$ ms followed by a 3D expansion of duration $t_{3D} = 18$ ms. Momentum distributions are measured by setting $t_{1D} = 0$ with the same t_{3D}. The magnetic field is switched to the imaging axis $\hat{y}$ at a time 5 ms after the start of the 3D expansion. To reduce the effect of initial gas size, we employ momentum focusing for measuring momentum distributions [8]. To determine the appropriate t_{1D} for the rapidity measurement, TOF density distributions with $t_{1D} = 0$–20 ms are measured; see Fig. 2. By $t_{1D} \approx 15$ ms, the distributions have asymptoted to the same shape, indicating that the density distribution reflects the rapidity distribution [5,14,15]. The inset also shows the saturation in the full width at half maximum (FWHM) of the distribution beyond 10–15 ms. For longer t_{1D}, imaging artifacts, stray magnetic field gradients, and lower signal-to-noise ratio degrade the image quality, as can be seen in the 20-ms data. We therefore use $t_{1D} = 15$ ms for the rapidity measurements.

Each 1D gas can be described by the Lieb-Liniger Hamiltonian [16] with the addition of an intratube DDI U_{DDI}^{1D} and a harmonic confining potential U_H,

$$H = \sum_{i=1}^{N}\left[-\frac{\hbar^2}{2m}\frac{\partial^2}{\partial x_i^2} + U_H(x_i)\right] + \sum_{1\leqslant i<j\leqslant N}\left[g_{1D}^{vdW}\delta(x_i - x_j) + U_{DDI}^{1D}(\theta_B, x_i - x_j)\right], \quad (1)$$

where m is the atomic mass, N is the number of atoms, and g_{1D}^{vdW} is the effective 1D contact interaction due to the van der Waals force; see Ref. [8]. Solving this Hamiltonian is very challenging because of the presence of the DDI term. To make theoretical progress, we account for only the leading-order,

short-range effect of the intratube DDI. (The intertube DDI is neglected.) Hence, we solve this 1D Hamiltonian after replacing $g_{1D}^{vdW} \to g_{1D} = g_{1D}^{vdW} + g_{1D}^{DDI}$ and setting $U_{DDI}^{1D}(\theta_B, x_i - x_j) = 0$ [8]. We note that the properties of the Lieb-Liniger model are parametrized by $\gamma = mg_{1D}/n_{1D}\hbar^2$, where n_{1D} is the 1D particle density. A $\gamma = 1$ denotes a strongly correlated Bose gas of intermediate-strength interactions, while $\gamma \to \infty$ indicates a TG gas, which can be mapped onto a system of noninteracting spinless fermions [1].

To model the experimental state preparation as closely as possible, we assume there is a lattice depth U_{2D}^* at which the 3D gas decouples into individual 1D gases as the 2D optical lattice is turned on [6]. At this lattice depth, we also assume that the 1D gases are in thermal equilibrium with each other at temperature T^* and at a global chemical potential that is set by the total number of particles. Then, using the local-density approximation (LDA) and the thermodynamic Bethe ansatz (TBA) [17], we determine N and the entropy of each 1D gas as functions of U_{2D}^* and T^*. As the depth of the 2D optical lattice is increased beyond U_{2D}^*, we assume that the 1D gases neither exchange particles nor interact. Thus, they no longer are in thermal equilibrium with each other. We assume this part of the loading process is adiabatic, i.e., that the entropy of each 1D gas is constant. We find the temperature of each 1D gas using (i) the number of atoms and entropies calculated at decoupling, and (ii) the experimental parameters measured at the end of the state preparation. The momentum and rapidity distributions are computed using these temperatures.

We compute the momentum distributions in the presence of the trap using path-integral quantum Monte Carlo with worm updates [18–20]. The rapidity distributions are computed within the LDA by solving the TBA equations. We then sum the results of the 1D gases to compare to the experimental absorption-imaging measurements (which provide distributions averaged over all 1D gases). The values of γ_T reported in the figures and throughout the text reflect the γ at which the LL model—at the experimentally set g_{1D} at *finite temperature*—exhibits the same ratio of kinetic-to-interaction energy obtained in our model at $\theta_B = 55°$ [8].

The free parameters in our model of state preparation are U_{2D}^* and T^*. We find the results to be rather insensitive to the precise value of U_{2D}^*, which suggests that assuming a single decoupling depth for all 1D gases is a reasonable approximation. We select $U_{2D}^* = 5E_R$ [8]. To find T^*, we minimize the quadrature sum of the differences between the experimental and theoretical momentum and rapidity distributions [8], which we call the "theoretical error." We plot this error for the results in the TG limit versus T^* in the inset of Fig. 3(a). We find the error minimum to be ∼5.5% at $T^* \approx 15$ nK. For $U_{2D}^* = 5E_R$ and $T^* \approx 15$ nK, we estimate the intertube DDI energy to be ∼4% of the kinetic+interaction plus trap energy of the 1D gases; see Ref. [8] for how intertube DDI energy is calculated. The comparison between the theoretical and experimental results for the momentum and rapidity distributions is shown in Fig. 3(a). The agreement is remarkable for the momentum distribution. The theoretical rapidity distribution is slightly narrower, which might be due in part to intertube DDI energy being converted into rapidity energy during the 1D expansion.

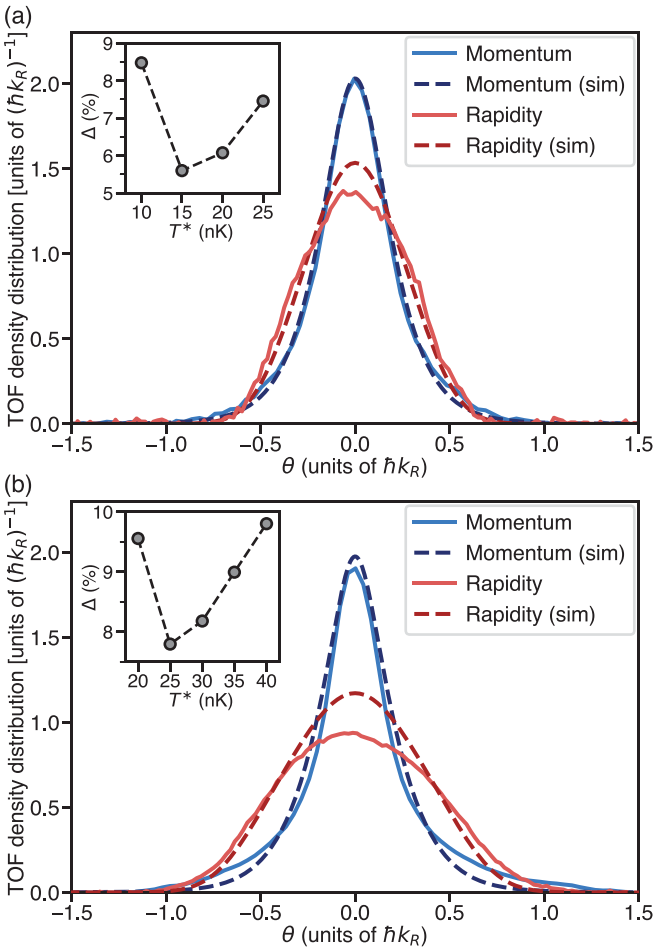

FIG. 3. Momentum and rapidity distributions; θ denotes either momentum or rapidity. Solid lines show the experimental momentum (blue) and rapidity (red) distributions, while the dashed lines show the simulation results. (a) Distributions for $\theta_B = 90°$ and $\gamma_T \approx 420$ in the TG limit. The simulations use $T^* = 15$ nK and $U_{2D}^* = 5E_R$. (b) Distributions for $\theta_B = 55°$ and $\gamma_T \approx 6.7$. Simulations use $T^* = 25$ nK and $U_{2D}^* = 5E_R$. Insets show the theoretical error used to select T^* [8].

Similarly, the comparison between experimental and theoretical results for the case of $\gamma_T \approx 6.7$ and $\theta_B = 55°$ is shown in Fig. 3(b). For these parameters, we estimate the intertube DDI energy to be ∼5.5% of the sum of kinetic, interaction, and trap energies of the 1D gases. The theoretical distributions follow the experimental ones, though less closely than in Fig. 3(a); they predict a lower occupation of high momenta and a narrower rapidity distribution.

Figure 4 reports our main results, the momentum and rapidity distributions of 1D dipolar quantum gases upon changing the contact and DDI strengths (and DDI sign). To reduce systematic variation, we always start from the same state—the one in Fig. 3(b)—when producing 1D gases with different interactions. That is, we begin with intratube nondipolar gases ($\theta_B = 55°$) at the background scattering length (yielding $\gamma_T \approx 6.7$) before we then change the magnetic field strength and θ_B to the desired final setting. No additional fitting is used to produce the theory curves because the number of atoms and entropies of the 1D gases at decou-

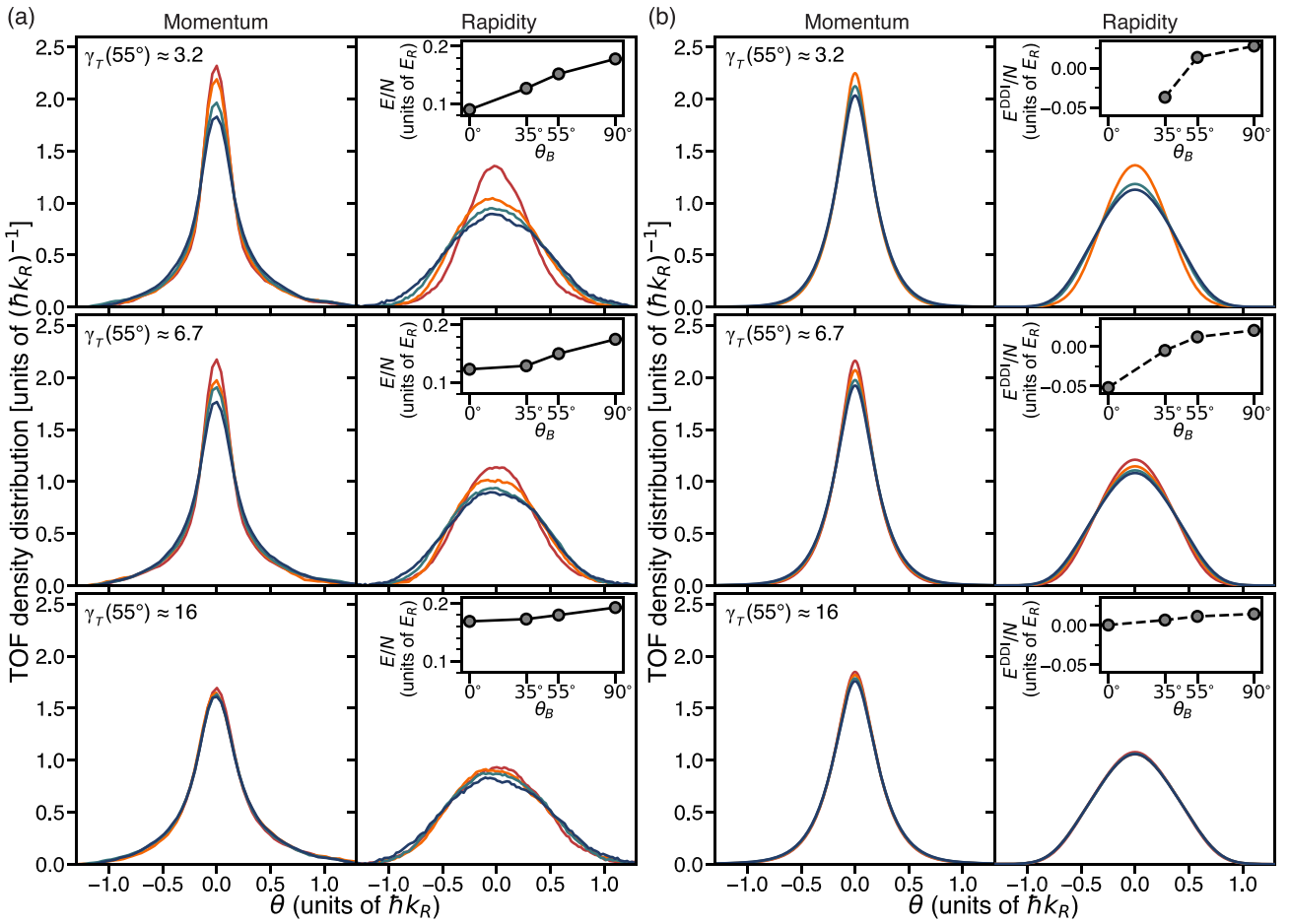

FIG. 4. (a) Measured momentum and rapidity distributions at field angles $\theta_B = 0°$ (red), 35° (orange), 55° (green), and 90° (blue) with $\gamma_T(\theta_B = 55°) \approx 3.2$, 6.7, and 16. θ denotes either momentum or rapidity. (b) Corresponding simulation curves. The insets in (a) show the total (interaction plus kinetic) energy that has been experimentally estimated from the rapidity distributions. Insets in (b) show the theoretically estimated total DDI energies, intertube plus short-range intratube. The θ_B dependence comes from the contribution to g_{1D} from the short-range part of the intratube 1D DDI. Note that the theory curves are missing for the case of $\gamma_T(55°) \approx 3.2$ and $\theta_B = 0°$ because g_{1D} becomes negative and we cannot simulate that regime.

pling were already computed. Hence, we need to calculate only the temperature of the 1D gases for the experimental parameters after the change in magnetic field angle and/or strength.

The experimental (theoretical) results are shown in Fig. 4(a) [Fig. 4(b)]. The experimentally observed broadening of the momentum and rapidity distributions for increasing γ_T at fixed θ_B and/or increasing θ_B at fixed γ_T is qualitatively captured by our theoretical model. It can be understood to be the result of increasing total (interaction plus kinetic) and kinetic energies through the increase of g_{1D} by way of the Feshbach resonance or short-range DDI.

We find that the rapidity and momentum distributions depend weakly on θ_B in the strongly correlated ($\gamma_T \approx 16$) TG regime. They exhibit larger changes versus θ_B as γ_T decreases. The insets in Fig. 4(a) show the changes with θ_B of the experimental estimation of the sum of the interaction and kinetic energies, calculated using the measured rapidity distributions. The insets in Fig. 4(b) show the changes with θ_B of our theoretical estimation of the total DDI energies, intertube plus short-range intratube. One can see that the changes in the total energy in the experiment become larger as γ_T decreases, and they parallel the larger changes observed in the estimated DDI energy. Our results illustrate how the nature of the equilibrium state changes as one tunes γ_T. When the contact interactions are strong, particles avoid each other and the 1D densities are lower, resulting in weaker dipolar interactions. As one decreases γ_T, particles in the equilibrium state of the integrable system are likelier to overlap; therefore, the 1D densities increase, and with them, the strength of the DDI. Remarkably, all these variations are accessible in our experimental apparatus.

In summary, we showed that the DDI significantly effects the equilibrium rapidity and momentum distributions of dipolar ^{162}Dy gases as one departs from the strongly correlated TG regime, suggesting that an increasingly stronger dressing of the quasiparticles takes place. Our model captured the main experimental trends, but quantitative differences remain. This is likely due in part to not accounting for the effect of the long-range aspect of the DDI. It couples different 1D gases as well as bosons that are far away within each 1D gas. The long-range DDI produce correlations and slow dynamical processes

that go beyond what can be computed using state-of-the-art numerical methods. Another potential source of discrepancy is the nonthermal effects related to the near integrability of the 1D gases as well as to heating, which we neglected. Nevertheless, it is remarkable that we are able to closely describe the experimental results in such a complex, strongly interacting system despite the above-mentioned omissions in our modeling. Notably, our largest "theoretical error" for the results reported in Fig. 4 is only ∼11%.

We hope our findings will motivate studies to incorporate the long-range part of the DDI in arrays of 1D gases described by otherwise integrable models [21], both to understand and quantify how they dress the quasiparticles in equilibrium and to clarify the role of near-integrability nonthermal effects during the initial state preparation. Such endeavors may usher a different direction for precision quantum many-body physics involving near-integrable models with short-range interactions perturbed by long-range interactions.

We thank Wil Kao for early experimental assistance and acknowledge the NSF (PHY-2006149) and AFOSR (FA9550-22-1-0366) for funding support. K.-Y. Lin acknowledges partial support from the Olympiad Scholarship from the Taiwan Ministry of Education. Y.Z. and M.R. acknowledge support from the NSF Grant No. PHY-2012145. S.G. acknowledges support from NSF DMR-2236517. Y.Z. acknowledges support from Dodge Family Postdoctoral Research Fellowship at the University of Oklahoma.

[1] M. A. Cazalilla, R. Citro, T. Giamarchi, E. Orignac, and M. Rigol, One dimensional bosons: From condensed matter systems to ultracold gases, Rev. Mod. Phys. **83**, 1405 (2011).

[2] Y. Tang, W. Kao, K.-Y. Li, S. Seo, K. Mallayya, M. Rigol, S. Gopalakrishnan, and B. L. Lev, Thermalization near Integrability in a Dipolar Quantum Newton's Cradle, Phys. Rev. X **8**, 021030 (2018).

[3] P. Calabrese, F. H. L. Essler, and G. Mussardo, Introduction to 'Quantum integrability in out of equilibrium systems', J. Stat. Mech. Theory Exp. (2016) 064001.

[4] L. Vidmar and M. Rigol, Generalized Gibbs ensemble in integrable lattice models, J. Stat. Mech.: Theory Exp. (2016) 064007.

[5] J. M. Wilson, N. Malvania, Y. Le, Y. Zhang, M. Rigol, and D. S. Weiss, Observation of dynamical fermionization, Science **367**, 1461 (2020).

[6] N. Malvania, Y. Zhang, Y. Le, J. Dubail, M. Rigol, and D. S. Weiss, Generalized hydrodynamics in strongly interacting 1D Bose gases, Science **373**, 1129 (2021).

[7] W. Kao, K.-Y. Li, K.-Y. Lin, S. Gopalakrishnan, and B. L. Lev, Topological pumping of a 1D dipolar gas into strongly correlated prethermal states, Science **371**, 296 (2021).

[8] See Supplemental Material at http://link.aps.org/supplemental/10.1103/PhysRevA.107.L061302 for information on experimental details and the numerical simulations.

[9] W. Kao, Y. Tang, N. Q Burdick, and B. L. Lev, Anisotropic dependence of tune-out wavelength near Dy 741-nm transition, Opt. Express **25**, 3411 (2017).

[10] L. Chomaz, I. Ferrier-Barbut, F. Ferlaino, B. Laburthe-Tolra, B. L. Lev, and T. Pfau, Dipolar physics: a review of experiments with magnetic quantum gases, Rep. Prog. Phys. **86**, 026401 (2023).

[11] M. Olshanii, Atomic Scattering in the Presence of an External Confinement and a Gas of Impenetrable Bosons, Phys. Rev. Lett. **81**, 938 (1998).

[12] E. Haller, M. J. Mark, R. Hart, J. G. Danzl, L. Reichsöllner, V. Melezhik, P. Schmelcher, and H.-C. Nägerl, Confinement-Induced Resonances in Low-Dimensional Quantum Systems, Phys. Rev. Lett. **104**, 153203 (2010).

[13] K. Baumann, N. Q. Burdick, M. Lu, and B. L. Lev, Observation of low-field Fano-Feshbach resonances in ultracold gases of dysprosium, Phys. Rev. A **89**, 020701(R) (2014).

[14] B. Sutherland, Exact Coherent States of a One-Dimensional Quantum Fluid in a Time-Dependent Trapping Potential, Phys. Rev. Lett. **80**, 3678 (1998).

[15] M. Rigol and A. Muramatsu, Fermionization in an Expanding 1D Gas of Hard-Core Bosons, Phys. Rev. Lett. **94**, 240403 (2005).

[16] E. H. Lieb and W. Liniger, Exact analysis of an interacting Bose gas. I. The general solution and the ground state, Phys. Rev. **130**, 1605 (1963).

[17] C. N. Yang and C. P. Yang, Thermodynamics of a one-dimensional system of bosons with repulsive delta-function interaction, J. Math. Phys. **10**, 1115 (1969).

[18] M. Boninsegni, N. Prokof'ev, and B. Svistunov, Worm Algorithm for Continuous-Space Path Integral Monte Carlo Simulations, Phys. Rev. Lett. **96**, 070601 (2006).

[19] M. Boninsegni, N. V. Prokof'ev, and B. V. Svistunov, Worm algorithm and diagrammatic Monte Carlo: A new approach to continuous-space path integral Monte Carlo simulations, Phys. Rev. E **74**, 036701 (2006).

[20] W. Xu and M. Rigol, Universal scaling of density and momentum distributions in Lieb-Liniger gases, Phys. Rev. A **92**, 063623 (2015).

[21] M. Panfil, S. Gopalakrishnan, and R. M. Konik, Thermalization of Interacting Quasi-One-Dimensional Systems, Phys. Rev. Lett. **130**, 030401 (2023).